Dynamic Rashba-Dresselhaus Effect

Martin Schlipf and Feliciano Giustino

Phys. Rev. Lett. **127**, 237601 — Published 2 December 2021

DOI: 10.1103/PhysRevLett.127.237601

Dynamic Rashba-Dresselhaus Effect

Martin Schlipf[1] and Feliciano Giustino[2,3,*]

[1] *VASP Software GmbH, Sensengasse 8, 1090 Vienna, Austria*
[2] *Oden Institute for Computational Engineering and Sciences, The University of Texas at Austin, Austin, Texas 78712, USA*
[3] *Department of Physics, The University of Texas at Austin, Austin, Texas 78712, USA*

(Dated: October 22, 2021)

The Rashba-Dresselhaus effect is the splitting of doubly degenerate band extrema in semiconductors, accompanied by the emergence of counter-rotating spin textures and spin-momentum locking. Here we investigate how this effect is modified by lattice vibrations. We show that, in centrosymmetric non-magnetic crystals, for which a bulk Rashba-Dresselhaus effect is symmetry-forbidden, electron-phonon interactions can induce a phonon-assisted, dynamic Rashba-Dresselhaus spin splitting in the presence of an out-of-equilibrium phonon population. In particular, we show how Rashba, Dresselhaus, or Weyl spin textures can selectively be established by driving coherent infrared-active phonons, and we perform *ab initio* calculations to quantify this effect for halide perovskites.

The interplay between crystal symmetry and spin-orbit coupling (SOC) is central to many phenomena in condensed matter physics, including multiferroicity [1, 2], topology [3], chirality [4, 5], the anomalous Hall effect [6], and skyrmions [7]. An important manifestation of SOC is the Rashba-Dresselhaus (RD) effect, whereby degenerate electron bands split and acquire counter-rotating spin orientations (Fig. 1) [8–11]. This effect can be used to generate and manipulate spin currents in Datta-Das transistors [12, 13], minimize spin dephasing in quantum devices [11, 14], and realize topological superconductivity and Majorana modes [15]. In current realizations, the RD effect is tuned electrically via a gate [13, 16] or chemically by balancing spin-orbit splitting and inversion-symmetry breaking [17]. Another theoretical possibility could be to induce this effect by dynamically breaking inversion symmetry [18–20].

In this work we develop the theory of dynamical control of the RD effect via phonon-assisted processes. To enable maximum tunability, we focus on non-magnetic centrosymmetric crystals, for which the RD effect is forbidden. We identify the phonon symmetry selection rules that lead to RD spin splitting with besopke Rashba, Dresselhaus, or Weyl spin textures, and we identify an *ab initio* descriptor to quantify this effect. As a first application, we calculate the dynamic RD effect for lead halide perovskites, and we show that it is within the detection range of current ultrafast experiments.

The RD effect can be understood starting from the standard SOC Hamiltonian:

$$V_{\mathrm{SOC}} = -\frac{e\,\hbar}{4m^2c^2}\,\mathbf{E}\cdot\boldsymbol{\sigma}\times\mathbf{p}\,, \tag{1}$$

where $\hbar$, e, m, c, $\boldsymbol{\sigma}$, and $\mathbf{p}$ denote Planck constant, electron charge and mass, speed of light, Pauli vector, and electron momentum, respectively. $\mathbf{E}$ is the electrostatic field experienced by the electrons. In the conventional Rashba effect one considers a uniform electric field along the Cartesian direction $\hat{z}$ as in Fig. 1(a), and a parabolic electron band with minimum at the Brillouin-zone center, so that V_{SOC} is proportional to $\sigma_x k_y - \sigma_y k_x$, where $\mathbf{k}$ is the Bloch wavevector of the electron. The related Dresselhaus coupling term is of the form $\sigma_x k_x - \sigma_y k_y$. The resulting band structures and spin textures are illustrated in Fig. 1(b) and (c)-(d), respectively.

In the absence of an external electric field, the vector $\mathbf{E}$ in Eq. (1) is replaced by the gradient of the single-particle potential energy, $\mathbf{E} = (1/e)\nabla V$, which depends parametrically on the atomic coordinates, for example the Kohn-Sham potential. Here, we ask the following question: under which conditions, in crystals with both space and time inversion symmetry, lattice vibrations can induce a dynamic RD effect via the dependence of V on the atomic positions.

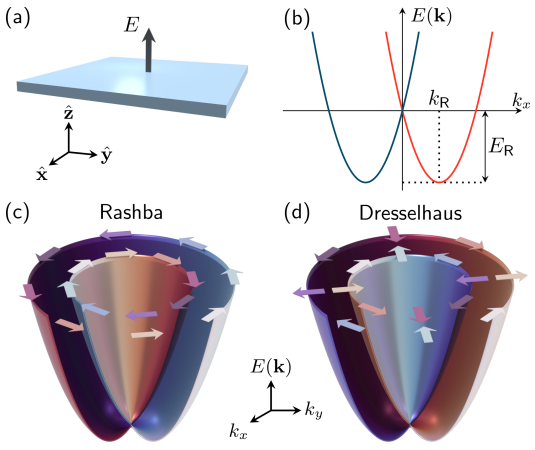

FIG. 1. (a) In the Rashba-Dresselhaus effect the inversion symmetry of the crystal is broken, for example by an electric field. This lifts the spin degeneracy of the band minimum. (b) As a result, the band minimum is lowered by the Rashba energy E_{R}, and is displaced by the Rashba wavevector k_{R}. Crystal symmetry dictates whether the system assumes a (c) Rashba or a (d) Dresselhaus spin texture as indicated by the color of the bands and the arrows.

To answer this question, we consider the phonon-induced spin-orbit coupling Hamiltonian in second-quantized notation:

$$\hat{V}_{\rm dRD} = N^{-\frac{1}{2}} \sum\nolimits_{\mathbf{k},\mathbf{q},s,s'} g_{s's}(\mathbf{k}{+}\mathbf{q},\mathbf{k})\, \hat{c}^\dagger_{\mathbf{k}+\mathbf{q}s'} \hat{c}_{\mathbf{k}s} (\hat{a}_{\mathbf{q}} {+} \hat{a}^\dagger_{-\mathbf{q}}) \,, \tag{2}$$

where $\mathbf{k}$ and $\mathbf{q}$ are electron and phonon wavevectors belonging to a uniform Brillouin zone grid with N points, $\hat{c}^\dagger_{\mathbf{k}s}/\hat{c}_{\mathbf{k}s}$ and $\hat{a}^\dagger_{\mathbf{q}}/\hat{a}_{\mathbf{q}}$ are creation/annihilation operators for electrons and phonons, respectively, and the subscript $s = 1, 2$ is the spinor label ('dRD' stands for 'dynamic RD'). The spin-phonon coupling matrix elements are:

$$g_{s's}(\mathbf{k}+\mathbf{q},\mathbf{k}) = \frac{\hbar}{4m_{\rm e}^2 c^2} \langle \psi_{\mathbf{k}+\mathbf{q}s'} | \boldsymbol{\sigma} \cdot \nabla(\Delta_{\mathbf{q}} V) \times \mathbf{p} \, | \psi_{\mathbf{k}s} \rangle \,, \tag{3}$$

where $\psi_{\mathbf{k}s}$ and $\psi_{\mathbf{k}+\mathbf{q}s'}$ are Pauli spinors, and $\Delta_{\mathbf{q}} V$ represents the variation of the potential when the ions undergo a collective displacement along the phonon eigenmode with wavevector $\mathbf{q}$. For notational simplicity we omit electron band and phonon branch indices; complete expressions are given in Supplementary Note 1 [21].

Thermal equilibrium – For a system with both time-reversal and inversion symmetry, it is intuitive that phonon-induced spin splitting must be forbidden in thermal equilibrium, because thermal fluctuations do not break space and time symmetries, as illustrated in Supplemental Fig. S1(a)-(c). Albeit intuitive, a rigorous proof of the lack of dynamic RD spin splitting in thermal equilibrium is nontrivial. Here we only sketch the key steps of the proof, leaving the complete analysis to Supplementary Notes 2 and 3.

We consider the degenerate states $|\pm\mathbf{k}, 1\rangle$ and $|\pm\mathbf{k}, 2\rangle$, obtained from the ground state $|0\rangle$ by creating an extra electron in the conduction band, $|\mathbf{k}s\rangle = \hat{c}^\dagger_{\mathbf{k}s}|0\rangle$. We analyze the effect of $\hat{V}_{\rm dRD}$ using many-body perturbation theory to all orders. Odd orders involve the diagonalization of terms that contains products of the matrix elements $\langle \mathbf{k}s | \hat{V}_{\rm dRD} | \mathbf{k}'s' \rangle$ with $s, s' = 1, 2$ and $\mathbf{k}' = \pm\mathbf{k}$. Each term of $\hat{V}_{\rm dRD}$ either creates or annihilates one phonon, therefore $\hat{V}_{\rm dRD}|\mathbf{k}'s'\rangle$ and $|\mathbf{k}s\rangle$ differ in their phonon occupations and the matrix elements vanish. Even orders (say $2n$-th) involve products of matrix elements in the form:

$$p_{s's} = \sum_{s_1} \sum_{s_2} \cdots \sum_{s_{2n-1}} g_{s's_1} g_{s_1 s_2} \cdots g_{s_{2n-1}s} \,, \tag{4}$$

where we omit electron momenta for clarity. In Supplementary Note 2 we show that parity and time-reversal symmetry require the matrix element to transform as follows under spin flip:

$$g_{\bar{s}'\bar{s}}(\mathbf{k}',\mathbf{k}) = (-1)^{s'-s+1} e^{i\varphi_{\mathbf{q}}}\, g^*_{s's}(\mathbf{k}',\mathbf{k}) \,, \tag{5}$$

where $\bar{s}$ is the spin label other than s, $\mathbf{q} = \mathbf{k}' - \mathbf{k}$, and $\varphi_{\mathbf{q}}$ is a phase associated with the transformation of vibrational eigenmodes upon inversion. Using Eq. (5) inside Eq. (4) we find $p_{\bar{s}'\bar{s}} = (-1)^{s'-s} p^*_{s's}$, hence $p^*_{12} = -p_{21}$. Since $\hat{V}_{\rm dRD}$ is Hermitian, we also have $p^*_{12} = p_{21}$, hence $p_{12} = p_{21} = 0$ and even-order terms vanish. In Supplementary Note 3 and 4 we analyze in detail the second-order and fourth-order energy shifts, and in Supplementary Note 5 we consider the case of finite temperature. This analysis confirms that phonons do not cause spin splitting in thermal equilibrium.

Out-of-equilibrium phonons – Next we move to a non-thermal phonon population. We focus on coherent Glauber states [Supplemental Fig. S1(d)], which can be generated and detected using ultrafast pump-probe techniques [22]. A coherent state associated with the phonon of momentum $\mathbf{q}$ and frequency $\omega_{\mathbf{q}}$ can be written as:

$$|\mathbf{k}s, u\rangle = \hat{c}^\dagger_{\mathbf{k}s} \exp(-Nu^2/2) \exp\big(N^{1/2} u\, \hat{a}^\dagger_{\mathbf{q}}\big)|0\rangle \,, \tag{6}$$

where $u(t)$ is the instantaneous fluctuation amplitude (this expression is for $\mathbf{q} = 0$; when $\mathbf{q} \neq 0$ the exponent is replaced by $\hat{a}^\dagger_{\mathbf{q}} + \hat{a}^\dagger_{-\mathbf{q}}$, see Supplementary Note 6). The instantaneous expectation value of the unperturbed Hamiltonian over this coherent state is $E_{\mathbf{k},u} = \varepsilon_{\mathbf{k}} + u^2 N\, \hbar\omega_{\mathbf{q}}$, where $\varepsilon_{\mathbf{k}}$ and $\omega_{\mathbf{q}}$ are the non-interacting electron energy and phonon frequency, respectively. Therefore u^2 quantifies the number of excited phonons per crystalline unit cell. Since $|\mathbf{k}s, u\rangle$ is an eigenvector of the annihilation operator $\hat{a}^\dagger_{\mathbf{q}}$, the expectation value of the atomic displacements $\Delta\boldsymbol{\tau}_\kappa$ on this state is nonzero:

$$\langle \Delta\boldsymbol{\tau}_\kappa \rangle_t = u(t)\, 2(\hbar/2M_\kappa\omega_{\mathbf{q}})^{1/2}\, \mathbf{e}_\kappa \,, \tag{7}$$

where M_κ is the mass of the κ-th atom, and $\mathbf{e}_\kappa$ is the phonon polarization. Unlike vibrations in thermal equilibrium, this state induces time-dependent inversion symmetry breaking.

To probe the consequences of symmetry breaking, we evaluate the instantaneous energy expectation value of the total Hamiltonian:

$$\langle \mathbf{k}s, u | \, \hat{H}_0 + \hat{V}_{\rm dRD} \, | \mathbf{k}s', u \rangle = \delta_{s's} E_{\mathbf{k},u} + 2\, \delta_{\mathbf{q},0}\, u\, g_{ss'}(\mathbf{k},\mathbf{k}) \,. \tag{8}$$

From the Kronecker delta $\delta_{\mathbf{q},0}$ we see that spin splitting is only allowed when $\mathbf{q} = 0$. This selection rule arises from the fact that only zone-center phonons can break the inversion symmetry of the crystal.

Time-reversal invariance implies that the vibrational eigenmodes can be chosen to satisfy $\mathbf{e}_\kappa(-\mathbf{q}) = \mathbf{e}^*_\kappa(\mathbf{q})$. Furthermore, invariance under parity requires $\mathbf{e}_{\tilde{\kappa}}(-\mathbf{q}) = -e^{i\varphi_{\mathbf{q}}} \mathbf{e}_\kappa(\mathbf{q})$, where the ion $\tilde{\kappa}$ is the inversion partner of κ, and $\varphi_{\mathbf{q}}$ is the same as in Eq. (5) [23]. For zone-center phonons, these relations imply that the eigenmodes have definite parity and $\varphi_{\mathbf{q}} = \pi \,/\, 0$ for even/odd phonons. Using this observation in Eq. (5), we obtain $g_{s\bar{s}}(\mathbf{k},\mathbf{k}) = \mp\, g_{s\bar{s}}(\mathbf{k},\mathbf{k})$ for even/odd phonons. It follows that spin splitting is allowed only for zone-center odd-parity modes.

To elucidate the nature of the spin-split bands, we diagonalize Eq. (8) by considering a parabolic band of mass m^* with extremum at the zone center. After performing a Taylor expansion of $g_{ss'}(\mathbf{k},\mathbf{k})$ at small $\mathbf{k}$, and noting that $g_{ss'}(0,0)=0$ as a consequence of inversion symmetry (see Supplementary Note 7), we obtain:

$$\Delta\varepsilon_{\mathbf{k}} = \pm 2E_{\mathrm{R}}\,|\mathbf{k}|/k_{\mathrm{R}}\ , \tag{9}$$

where the Rashba energy and wavevectors are $E_{\mathrm{R}} = \hbar^2 k_{\mathrm{R}}^2/2m^*$ and $k_{\mathrm{R}} = \|\hat{\mathbf{k}}\cdot\nabla_{\mathbf{k}}\, g_{ss'}(\mathbf{k},\mathbf{k})\|u\sqrt{2}m^*/\hbar^2$, respectively. Here $\hat{\mathbf{k}} = \mathbf{k}/|\mathbf{k}|$ and $\|\cdot\|$ is the Frobenius norm in the spin indices. Eq. (9) shows that the splitting vanishes at $\mathbf{k}=0$, and increases linearly with $\mathbf{k}$ away from the zone center. This is precisely the hallmark of the Rashba effect encoded in Eq. (1). The resulting electronic bands are sketched in Fig. 1(c). In the case of driven oscillations, the splitting and the associated spin texture will fluctuate with the amplitude $u(t)$.

In Supplementary Note 8 we show that that the Rashba energy in Eq. (9) for the Fröhlich interaction associated with longitudinal-optical (LO) phonons in polar crystals [24] is negligible. Combined with the fact that only transverse-optical (TO) modes are excited by light in bulk crystals, this result suggests that the search for a dynamic RD effect should focus on zone-center TO modes of ungerade (u) symmetry, namely the IR-active modes of polar crystals. Since in centrosymmetric crystals the modes cannot simultaneously be IR- and Raman- active, we must rule out the possibility of directly realizing RD splitting using a Raman-active mode (unless the Raman mode is used to excite an IR mode via nonlinear couplings [25]).

To examine the spin texture associated with the above RD splitting, we consider the symmetry of the spin-phonon matrix element in Eq. (3). Let us call $\mathbf{g}$ the 2×2 matrix with elements $g_{ss'}(\mathbf{k},\mathbf{k})$ in the spinor labels s,s'. Using $\mathbf{k}\cdot\mathbf{p}$ perturbation theory and the algebra of Pauli matrices, in Supplementary Note 9 we show that $\mathbf{g}$ can be expressed as:

$$\mathbf{g} = \sum_{\alpha\beta} k_\alpha G_{\alpha\beta}\,\sigma_\beta\ , \tag{10}$$

where the components of the real-valued 3×3 matrix $G_{\alpha\beta}$ take the form $G_{11} = (\hbar^2/8m_e^2c^2)\langle 0,1|[\boldsymbol{\sigma}\times\nabla]_\alpha\Delta_0 V)|0,2\rangle$ + c.c. , and similarly for the other elements. The complete matrix is given in Supplementary Note 9, Eq. (S81). Direct inspection of Eq. (10) shows that the isotropic part of $G_{\alpha\beta}$ leads to couplings like $k_x\sigma_x + k_y\sigma_y + k_z\sigma_z$, and therefore it induces a Weyl spin texture. The traceless symmetric part of $G_{\alpha\beta}$ leads to couplings like $k_x\sigma_x - k_y\sigma_y$ or $k_x\sigma_y + k_y\sigma_x$, hence it induces a Dresselhaus spin texture. The antisymmetric part of $G_{\alpha\beta}$ leads to couplings like $k_x\sigma_y - k_y\sigma_x$, which correspond to a Rashba spin texture. Altogether, the present findings indicate that a dynamic RD effect with similar phenomenology as the conventional (static) effect is theoretically possible, and that the spin texture can be tuned by exciting IR modes of select symmetry.

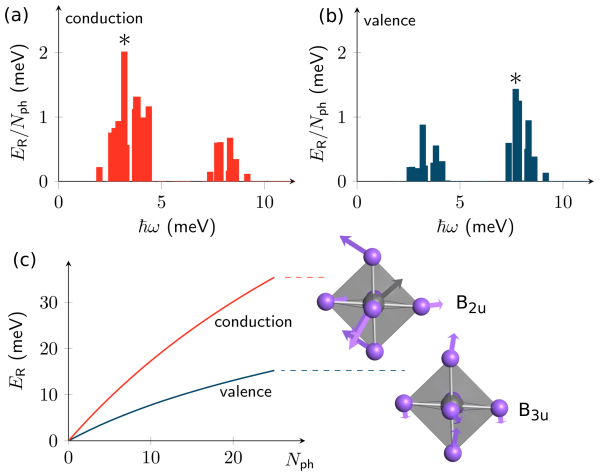

FIG. 2. (a) Rashba energy for every IR-active mode in MAPI and for the conduction band bottom. The energy is evaluated for $N_{\mathrm{ph}} = u^2 = 1$ excited phonon per orthorhombic unit cell. (b) Same as in (a), but for the valence band of MAPI. (c) Dependence of the Rashba energy on the number of phonons per unit cell excited in the modes marked by asteriscs in (a) and (b): the $B_{2\mathrm{u}}$ Pb-I-Pb rocking mode at 3.2 meV, and the $B_{3\mathrm{u}}$ Pb-I stretching mode at 7.7 meV. These modes are schematically illustrated by the ball-and-stick models.

Proposed experiments – To realize a dynamic RD effect using out-of-equilibrium coherent phonons, we propose to perform THz pump/optical probe experiments on halide perovskites, following recent work on methylammonium lead iodide (MAPI, $CH_3NH_3PbI_3$) [20, 26, 27] which is known to have a large SOC [28]. Below 160 K MAPI crystallizes in a orthorhombic structure with centrosymmetric space group *Pnma* (Supplementary Fig. S4). This system admits 20 IR-active optical phonons, associated with the deformation of the PbI_6 octahedra [29]. Figure 2 shows the Rashba energy E_{R} for each of these modes, as calculated using Eq. (9). For the conduction band, we find that the $B_{2\mathrm{u}}$ mode at 3.2 meV, which corresponds to the Pb-I-Pb rocking vibration, provides the largest spin splitting [Fig. 2(a)]. For the valence bands, the largest splitting is found with the $B_{3\mathrm{u}}$ mode at 7.7 meV, corresponding to the Pb-I stretching vibration [Fig. 2(b)].

The maximum RD splitting achievable in experiments is limited by the stability of the crystal under illumination. According to Lindemann's criterion [30], melting occurs when the ionic displacements exceed approximately 10% of the equilibrium bond length. An upper bound to the displacement in Eq. (7) is $\Delta\tau_{\max} = 2(N_{\mathrm{ph}}\hbar/2M_{\min}\omega_{\mathbf{q}})^{1/2}$, where $M_{\min}$ is the smallest atomic mass. Using the mass of iodine and the frequency of the $B_{2\mathrm{u}}$ mode, and setting $\Delta\tau_{\max}$ to 10% of the Pb-I

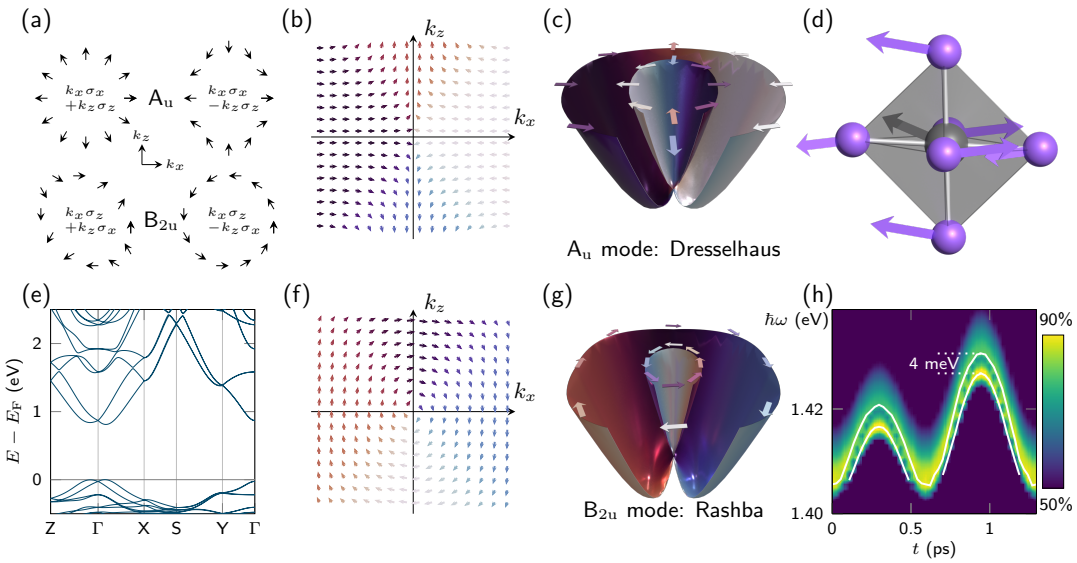

FIG. 3. (a) Allowed spin textures in the k_x-k_z plane for A_u and B_{2u} modes. The A_u mode is compatible with a Weyl or Dresselhaus texture, the B_{2u} mode admits a Dresselhaus or Rashba texture. (b)-(c) Upon driving the A_u mode, the spin texture of the conduction band assumes a Dresselhaus pattern, similar to Fig 1(d). The ball-and-stick model of this mode is shown in (d). (e) Spin-split band structure resulting from coherently driving the B_{2u} mode in MAPI. (f)-(g) Driving the B_{2u} mode results into a Rashba spin texture, similar to Fig 1(c). (b) and (f) show the spin texture for the conduction band bottom projected on the k_x-k_z plane. (c) and (g) show the spin texture color-coded on the band structure. (h) The RD band splitting associated with a periodically driven B_{2u} mode induces a fluctuating peak-dip-hump structure in the PL spectrum of MAPI.

bond length (3.2 Å), we find $N_{\rm ph} = 50$. Figure 2(c) shows that, even for considerably smaller vibrational amplitudes, Rashba energies in excess of 30 meV should be within reach.

A representative band structure snapshot corresponding to the B_{2u} mode is shown in Fig. 3(a). These bands describe the system at a given time t. Since the B_{2u} mode oscillates with a period of 1.3 ps, and the electron lifetime near the conduction band edges of MAPI is ∼10 fs at 160 K [31], electrons effectively experience a quasi-static potential. Therefore the notion of 'instantaneous' bands is meaningful in this case.

The spin textures for the A_u and B_{2u} excitations are shown in Fig. 3(b), (c), (f), and (g). To understand the spin patterns, let us consider the elements of the matrix G in Eq. (10) for odd-parity modes in the D_{2h} point group. If Γ_α is the irreducible representation of the operator $[\boldsymbol{\sigma} \times \nabla]_\alpha(\Delta_0 V)$ appearing in Eq. (10), group theory [32] determines which matrix elements of $G_{\alpha\beta}$ can be nonzero. Using Supplementary Table S1 A, we find that for any given representation Γ_α only a single component β yields a nonzero element. In particular, these are $\beta = 3$ ($\Gamma_\alpha = B_{1g}$), $\beta = 2$ ($\Gamma_\alpha = B_{2g}$), and $\beta = 1$ ($\Gamma_\alpha = B_{3g}$), which is exactly the representation of σ_β as expected. Next, we need to determine Γ_α for a given phonon mode. In Supplementary Table S1 B we give the product of the irreducible representations of Pauli matrix, gradient, and phonon mode for the different Cartesian directions, and we indicate the resulting allowed couplings between $\mathbf{k}$ and $\boldsymbol{\sigma}$, corresponding to nonzero elements of the matrix $G_{\alpha\beta}$. This analysis indicates that the allowed couplings correspond to $k_x\sigma_x$, $k_y\sigma_y$, $k_z\sigma_z$ for the A_u mode, $k_x\sigma_y$, $k_y\sigma_x$ for the B_{1u} mode with polarization along z, $k_x\sigma_z$, $k_z\sigma_x$ for the B_{2u} mode with polarization along y, and $k_y\sigma_z$, $k_z\sigma_y$ for the B_{3u} mode with polarization along x. The orthorhombic symmetry does not dictate the sign relationships between the allowed couplings, so the signs must be determined by direct inspection of the spin texture. In Fig. 3(e) we show that a B_{2u} mode is compatible with a Rashba or Dresselhaus spin pattern and the A_u mode with a Weyl or Dresselhaus texture. By manually inspecting the spin patterns we confirm that our *ab initio* calculations follow the above symmetry considerations: For the A_u mode a Dresselhaus pattern is established [Fig. 3(b) and (c)], whereas the B_{2u} mode leads to a Rashba pattern [Fig. 3(f) and (g)].

The key experimental challenge to realize the dynamic RD effect proposed here, is to pump coherent oscillations in the low-THz range (the B_{2u} mode of MAPI has a frequency ∼0.8 THz) without damaging the sample [33, 34]. A promising approach that has emerged during the past few years is to exploit resonant sum-frequency excitation processes [22, 33]. This approach was demonstrated for Te crystals (2 THz source) [34], $SrTiO_3$ (3 THz) [35], Bi_2Se_3 (1 THz) [36], $LiNbO_3$ (1 THz, 4 THz, and 18 THz) [37–39], and $CdWO_4$ (2 THz) [40]. More recently, single-cycle THz pulses have been used to drive coherent oscillations in MAPI [26]. In his work, the au-

thors were able to detect coherent oscillations in the differential reflectivity spectra lasting as long as 5 ps, which should be more than sufficient to realize the effect proposed here.

A possible way to probe the driven dynamic RD effect would be via time-resolved ARPES experiments. In such experiments the shape of the constant-energy cuts should oscillate between a circle in absence of RD splitting, as observed in Ref. 41, and two distinct circles for Rashba-split bands. Alternatively one could monitor optical properties such as the oscillator strength of the first excitonic peak [42], which is expected to be sensitive to the fluctuating RD splitting of the band extrema [26]. As an illustrative example, we have calculated the time-revolved photoluminescence (PL) spectrum of MAPI with the B_{2u} coherently driven (see Supplementary Methods). Fig. 3(h) shows that the dynamic RD effect induces a discernible fluctuating peak-dip-hump structure in the PL signal.

In summary, we developed an *ab initio* theory of the dynamic, phonon-assisted Rashba-Dresselhaus effect and proposed experimental realizations. We showed that, in centrosymmetric non-magnetic crystals, it is possible to establish a spin splitting with Rashba, Dresselhaus, or Weyl spin texture by driving coherent oscillations of infrared-active optical modes of select symmetry. Our work shows that phonons may provide new strategies for harnessing the spin degrees of freedom in quantum materials.

This work was supported by the Computational Materials Sciences Program funded by the U.S. Department of Energy, Office of Science, Basic Energy Sciences, under Award DE-SC0020129 (project design, theory development, manuscript preparation) and the Leverhulme Trust under award RL-2012-001 (theory development, *ab initio* calculations, manuscript preparation). The authors acknowledge the Texas Advanced Computing Center (TACC) at The University of Texas at Austin for providing HPC resources via the Frontera LRAC project DMR21002.

* fgiustino@oden.utexas.edu

[1] M. Kenzelmann, A. B. Harris, S. Jonas, C. Broholm, J. Schefer, S. B. Kim, C. L. Zhang, S. W. Cheong, O. P. Vajk, and J. W. Lynn, Phys. Rev. Lett. **95**, 087206 (2005).
[2] S.-W. Cheong and M. Mostovoy, Nat. Mater. **6**, 13 (2007).
[3] M. Z. Hasan and C. L. Kane, Rev. Mod. Phys. **82**, 3045 (2010).
[4] Z. K. Liu, B. Zhou, Y. Zhang, Z. J. Wang, H. M. Weng, D. Prabhakaran, S.-K. Mo, Z. X. Shen, Z. Fang, X. Dai, Z. Hussain, and Y. L. Chen, Science **343**, 864 (2014).
[5] S.-Y. Xu, I. Belopolski, N. Alidoust, M. Neupane, G. Bian, C. Zhang, R. Sankar, G. Chang, Z. Yuan, C.-C. Lee, S.-M. Huang, H. Zheng, J. Ma, D. S. Sanchez, B. Wang, A. Bansil, F. Chou, P. P. Shibayev, H. Lin, S. Jia, and M. Z. Hasan, Science **349**, 613 (2015).
[6] N. Nagaosa, J. Sinova, S. Onoda, A. H. MacDonald, and N. P. Ong, Rev. Mod. Phys. **82**, 1539 (2010).
[7] A. Fert, N. Reyren, and V. Cros, Nat. Rev. Mater. **2**, 17031 (2017).
[8] E. Rashba, J. Electron. Spectrosc. **201**, 4 (2015).
[9] G. Dresselhaus, Phys. Rev. **100**, 580 (1955).
[10] G. Bihlmayer, O. Rader, and R. Winkler, New J. Phys. **17**, 050202 (2015).
[11] A. Manchon, H. C. Koo, J. Nitta, S. M. Frolov, and R. A. Duine, Nat. Mater. **14**, 871 (2015).
[12] S. Datta and B. Das, Appl. Phys. Lett. **56**, 665 (1990).
[13] H. C. Koo, J. H. Kwon, J. Eom, J. Chang, S. H. Han, and M. Johnson, Science **325**, 1515 (2009).
[14] I. Žutić, J. Fabian, and S. Das Sarma, Rev. Mod. Phys. **76**, 323 (2004).
[15] S. Kezilebieke, M. N. Huda, V. Vaňo, M. Aapro, S. C. Ganguli, O. J. Silveira, S. Glodzik, A. S. Foster, T. Ojanen, and P. Liljeroth, Nature **588**, 424 (2020).
[16] J. Wunderlich, B.-G. Park, A. C. Irvine, L. P. Zârbo, E. Rozkotová, P. Nemec, V. Novák, J. Sinova, and T. Jungwirth, Science **330**, 1801 (2010).
[17] V. Sunko, H. Rosner, P. Kushwaha, S. Khim, F. Mazzola, L. Bawden, O. Clark, J. Riley, D. Kasinathan, M. Haverkort, T. Kim, M. Hoesch, J. Fujii, I. Vobornik, A. Mackenzie, and P. King, Nature **549**, 492496 (2017).
[18] T. Etienne, E. Mosconi, and F. De Angelis, J. Phys. Chem. Lett. **7**, 1638 (2016).
[19] B. Monserrat and D. Vanderbilt, arXiv:1711.06274 (2017).
[20] D. Niesner, M. Hauck, S. Shrestha, I. Levchuk, G. J. Matt, A. Osvet, M. Batentschuk, C. Brabec, H. B. Weber, and T. Fauster, Proc. Natl. Acad. Sci. USA **115**, 9509 (2018).
[21] See Supplemental Notes 1-9 for detailed derivations, and Supplemental Table S1 and Figs. S1-S4 at [URL], which includes Refs. 23, 24, 32, 43–62.
[22] P. Salén, M. Basini, S. Bonetti, J. Hebling, M. Krasilnikov, A. Y. Nikitin, G. Shamuilov, Z. Tibai, V. Zhaunerchyk, and V. Goryashko, Phys. Rep. **836**, 1 (2019).
[23] A. A. Maradudin and S. H. Vosko, Rev. Mod. Phys. **40**, 1 (1968).
[24] H. Fröhlich, Adv. Phys. **3**, 325 (1954).
[25] P. G. Radaelli, Phys. Rev. B **97**, 085145 (2018).
[26] Z. Liu, C. Vaswani, X. Yang, X. Zhao, Y. Yao, Z. Song, D. Cheng, Y. Shi, L. Luo, D.-H. Mudiyanselage, C. Huang, J.-M. Park, R. H. J. Kim, J. Zhao, Y. Yan, K.-M. Ho, and J. Wang, Phys. Rev. Lett. **124**, 157401 (2020).
[27] K. Frohna, T. Deshpande, J. Harter, W. Peng, B. A. Barker, J. B. Neaton, S. G. Louie, O. M. Bakr, D. Hsieh, and M. Bernardi, Nat. Commun. **9**, 1829 (2018).
[28] J. Even, L. Pedesseau, J. Jancu, and C. Katan, J. Phys. Chem. Lett. **4**, 2999 (2013).
[29] M. A. Pérez-Osorio, R. L. Milot, M. R. Filip, J. B. Patel, L. M. Herz, M. B. Johnston, and F. Giustino, J. Phys. Chem. C **119**, 25703 (2015).
[30] F. Lindemann, Z. Phys **11**, 609 (1910).
[31] M. Schlipf, S. Poncé, and F. Giustino, Phys. Rev. Lett. **121**, 086402 (2018).
[32] G. F. Koster, J. O. Dimmock, R. G. Wheeler, and

H. Statz, *M.I.T. Press research monographs No. 34* (M.I.T. Press, Cambridge, Mass., 1963).
[33] M. Udina, T. Cea, and L. Benfatto, Phys. Rev. B **100**, 165131 (2019).
[34] T. Huber, M. Ranke, A. Ferrer, L. Huber, and S. L. Johnson, Appl. Phys. Lett. **107**, 091107 (2015).
[35] M. Kozina, T. van Driel, M. Chollet, T. Sato, J. M. Glownia, S. Wandel, M. Radovic, U. Staub, and M. C. Hoffmann, Struct. Dyn. **4**, 054301 (2017).
[36] A. A. Melnikov, K. N. Boldyrev, Y. G. Selivanov, V. P. Martovitskii, S. V. Chekalin, and E. A. Ryabov, Phys. Rev. B **97**, 214304 (2018).
[37] H. Hirori, A. Doi, F. Blanchard, and K. Tanaka, Appl. Phys. Lett. **98**, 091106 (2011).
[38] B. S. Dastrup, J. R. Hall, and J. A. Johnson, Appl. Phys. Lett. **110**, 162901 (2017).
[39] A. von Hoegen, R. Mankowsky, M. Fechner, M. Först, and A. Cavalleri, Nature **555**, 79 (2018).
[40] C. L. Johnson, B. E. Knighton, and J. A. Johnson, Phys. Rev. Lett. **122**, 073901 (2019).
[41] M. Puppin, S. Polishchuk, N. Colonna, A. Crepaldi, D. N. Dirin, O. Nazarenko, R. De Gennaro, G. Gatti, S. Roth, T. Barillot, L. Poletto, R. P. Xian, L. Rettig, M. Wolf, R. Ernstorfer, M. V. Kovalenko, N. Marzari, M. Grioni, and M. Chergui, Phys. Rev. Lett. **124**, 206402 (2020).
[42] C. L. Davies, M. R. Filip, J. B. Patel, T. W. Crothers, C. Verdi, A. D. Wright, R. L. Milot, F. Giustino, M. B. Johnston, and L. M. Herz, Nat. Commun. **9**, 1 (2018).
[43] T. Baikie, Y. Fang, J. M. Kadro, M. Schreyer, F. Wei, S. G. Mhaisalkar, M. Graetzel, and T. J. White, J. Mater. Chem. A **1**, 5628 (2013).
[44] S. Baroni, S. de Gironcoli, A. Dal Corso, and P. Giannozzi, Rev. Mod. Phys. **73**, 515 (2001).
[45] P. Giannozzi, O. Andreussi, T. Brumme, O. Bunau, M. B. Nardelli, M. Calandra, R. Car, C. Cavazzoni, D. Ceresoli, M. Cococcioni, N. Colonna, I. Carnimeo, A. D. Corso, S. de Gironcoli, P. Delugas, R. DiStasio, A. Ferretti, A. Floris, G. Fratesi, G. Fugallo, R. Gebauer, U. Gerstmann, F. Giustino, T. Gorni, J. Jia, M. Kawamura, H.-Y. Ko, A. Kokalj, E. Küçükbenli, M. Lazzeri, M. Marsili, N. Marzari, F. Mauri, N. L. Nguyen, H.-V. Nguyen, A. O. de-la Roza, L. Paulatto, S. Poncé, D. Rocca, R. Sabatini, B. Santra, M. Schlipf, A. P. Seitsonen, A. Smogunov, I. Timrov, T. Thonhauser, P. Umari, N. Vast, X. Wu, and S. Baroni, J. Phys.: Condens. Matter **29**, 465901 (2017).
[46] D. Vanderbilt, Phys. Rev. B **41**, 7892 (1990).
[47] J. P. Perdew, K. Burke, and M. Ernzerhof, Phys. Rev. Lett. **77**, 3865 (1996).
[48] H. T. Stokes, D. M. Hatch, and B. J. Campbell, "ISOTROPY Software Suite," `http://iso.byu.edu` (2020).
[49] F. Giustino, Rev. Mod. Phys. **89**, 015003 (2017).
[50] P. Yu and M. Cardona, *Fundamentals of Semiconductors*, 4th ed. (Springer-Verlag, Berlin, 2010).
[51] L. I. Schiff, *Quantum Mechanics*, 3rd ed. (McGraw-Hill, New York, 1968).
[52] L. D. Landau and E. M. Lifshitz, *Quantum Mechanics: Non-Relativistic Theory*, 3rd ed. (Elsevier, Oxford, 1981).
[53] J. R. Schrieffer, *Theory of Superconductivity*, Advanced Book Program Series (Perseus, 1983).
[54] G. D. Mahan, *Many-Particle Physics*, 2nd ed. (Plenum, New York, 1993).
[55] D. J. Scalapino, "The electron-phonon interaction and strong-coupling superconductors," (Routledge, New York, 1969) p. 449.
[56] G. Grimvall, *The electron-phonon interaction in metals* (North-Holland, Amsterdam, 1981).
[57] C. Cohen-Tannoudji, B. Diu, and F. Laloe, *Quantum Mechanics* (Wiley, 1977).
[58] W. H. Sio, C. Verdi, S. Poncé, and F. Giustino, Phys. Rev. B **99**, 235139 (2019).
[59] A. Miyata, A. Mitioglu, P. Plochocka, O. Portugall, J. T.-W. Wang, S. D. Stranks, H. J. Snaith, and R. J. Nicholas, Nat. Phys. **11**, 582 (2015).
[60] M. Hirasawa, T. Ishihara, T. Goto, K. Uchida, and N. Miura, Physica B **201**, 427 (1994).
[61] A. Poglitsch and D. Weber, J. Chem. Phys. **87**, 6373 (1987).
[62] P. Whitfield, N. Herron, W. Guise, K. Page, Y. Cheng, I. Milas, and M. Crawford, Sci. Rep. **6**, 35685 (2016).